Modeling and quantitative nanocalorimetric analysis to assess interdiffusion in a Ni/Al bilayer

M. Vohra, M. Grapes, P. Swaminathan, T. P. Weihs, and O. M. Knio

Citation: Journal of Applied Physics **110**, 123521 (2011); doi: 10.1063/1.3671639
View online: http://dx.doi.org/10.1063/1.3671639
View Table of Contents: http://scitation.aip.org/content/aip/journal/jap/110/12?ver=pdfcov
Published by the AIP Publishing

Modeling and quantitative nanocalorimetric analysis to assess interdiffusion in a Ni/Al bilayer

M. Vohra,[1] M. Grapes,[2] P. Swaminathan,[2] T. P. Weihs,[2] and O. M. Knio[1,a)]
[1]*Department of Mechanical Engineering, Johns Hopkins University Baltimore, Maryland 21218, USA*
[2]*Department of Materials Science and Engineering, Johns Hopkins University Baltimore, Maryland 21218, USA*

(Received 17 September 2011; accepted 19 November 2011; published online 23 December 2011)

A computational model is developed to describe the evolution of the temperature field in a nanocalorimeter that comprises inert material layers on which a nanoscale Ni/Al bilayer has been deposited. The model incorporates a reduced continuum description of mixing and heat release in the Ni/Al bilayer, and of the energy equation in the inert layers. Due to the small thicknesses of individual layers that are several orders of magnitude smaller than the corresponding length, a simplified, transient, homogeneous representation of the temperature field can be adopted. The resulting lumped model is valid over short enough timescales, which are nonetheless sufficiently large to capture the formation reaction. By using experimental observations of the evolution of the temperature on the surface of the nanocalorimeter, the model is used to estimate the transient heat release rate. Assuming an Arrhenius model for the mixing between Ni and Al, the estimated heat release rate is used to determine the Arrhenius pre-exponent and activation energy of the atomic diffusivity. Computed results indicate that the present approach provides a promising means of characterizing atomic diffusion rates. Limitations arise, however, due to the low amplitudes of the heat release term at low temperature, and also due to phase-change effects, which make the heat release rate unobservable in the neighborhood of the melting temperature of individual constituents. For the present system, reliable estimates are extracted for temperatures ranging from about 600 K to the Al melting temperature. © *2011 American Institute of Physics*. [doi:10.1063/1.3671639]

I. INTRODUCTION

Nanocalorimetry is a chip-based measurement of thermal and thermodynamic phenomena taking place within nanoscale material samples. When used in conjunction with fast scanning instruments, nanocalorimetry offers the possibility of resolving phenomena at times scales that are several orders of magnitude smaller than is possible with conventional nanocalorimetry. This paper specifically focuses on exploring, computationally, the potential of using temperature measurements obtained using a differential scanning nanocalorimeter[1,2] in order to quantify the heat release in a reactive Ni/Al bilayer, and consequently infer instantaneous mixing rates and their temperature dependence.

The experimental data used as input to the present study have been obtained using the nanocalorimeter design illustrated in Fig. 1. As illustrated in the sketch, the nanocalorimeter comprises a stack of nanoscale layers that are deposited onto a silicon nitride substrate. On the top side of the substrate, the stack features a 3 nm-thick Ti layer and a 50 nm-thick Pt layer; on the bottom side, the stack features a Ni/Al bilayer having with a 1:1 ratio of the elements, which is embedded within two, 10 nm-thick, alumina layers. The Pt layer was deposited by e-beam evaporation; the measured values of heat capacity and density were found to be consistent with bulk values. The device operates by driving a current through the stack, with pulse duration on the order of tens of milliseconds. The current and voltage across the stack are also recorded during the pulse; a four-point probe was used for this purpose. The temperature on the Pt surface is determined from the temperature versus resistance calibration obtained using a one-color, optical pyrometer operating at 1550 nm. The error in the temperature measurement was found to be 2.5 °C. Thus, available experimental inputs include the time histories of the current and voltage across the stack, and the temperature at the Pt surface. Typical currents are less than 100 mA. With a stack cross of 0.5 mm × 6 mm, the current density is approximately 30 000 A/m^2. Consequently, electromigration is not expected to be significant. Details on the construction of the nanocalorimeter and on measurement techniques will be provided elsewhere.[3]

With an increase in temperature due to Joule heating, intermixing between Ni and Al occurs at increasingly higher rates. This highly exothermic process leads to additional heating within the stack, at least until the reaction between Ni and Al is fully complete. Note that on time scales on the order of the current pulse, the thermal penetration width is of the order of hundreds of microns and hence is by several orders of magnitude larger than the thickness of the stack, whereas it is substantially smaller than the stack length which is of the order of millimeters. This implies that temperature is essentially uniform across the thickness of the stack, and that it is also uniform over substantially most of the stack length. Thus, the reaction in the Ni/Al bilayer occurs in an essentially spatially homogeneous fashion.

a)Author to whom correspondence should be addressed. Present address: Department of Mechanical Engineering and Materials Science, Duke University, Durham, NC 27708, USA. Electronic mail: omar.knio@duke.edu.

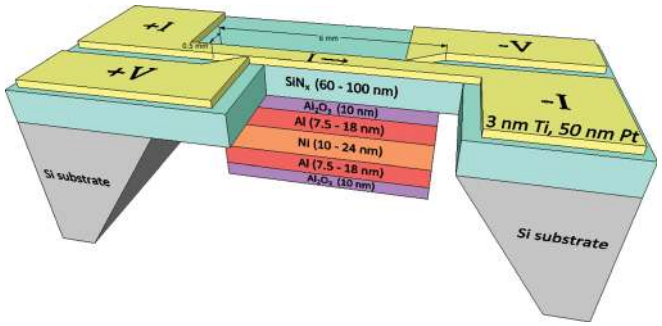

FIG. 1. (Color online) Schematic illustration of a multilayer configuration found in a typical nanocalorimeter. Also, shown are the leads for 4-pt current and voltage drop measurement.

This reaction regime offers an interesting approach to characterizing mixing and reaction in multilayer materials, which complements prior attempts that have primarily relied on conventional differential scanning calorimetry[4,5] or on observations of self-propagating reaction fronts.[6–18] Advantageous features afforded by the present approach include fast, time resolved measurements, and the homogeneous nature of the reaction which leads to simplified models and circumvents the need for accurate representation of conductive heat fluxes.[19]

This paper develops a simplified model of the evolution of the temperature within nanocalorimeter stacks similar to that depicted in Fig. 1. An outline of the development of the simplified model is given in Sec. II. The thermal model is then exploited in Sec. III in order to develop a procedure for inferring the atomic diffusivity based on the measured voltage and current across the stack, and on the measured temperature. As discussed in Ref. 3, the latter is determined using a temperature versus resistance correlation, obtained using a pyrometer. This analysis is then applied in Sec. IV to estimate the diffusivity and characterize its dependence on the temperature. The results are then used to estimate the parameters of the Arrhenius diffusivity law assumed by the Ni/Al reaction model. Major conclusions are given in Sec. V.

II. THERMAL MODEL

A simplified thermal model for the evolution of the temperature within the nanocalorimeter is developed for the small-time limit. In this limit, the temperature within the nanocalorimeter can be treated as spatially homogeneous, and its evolution is governed by the volume averaged energy conservation equation

$$V\frac{\partial H}{\partial t} = \mathcal{V}\dot{Q} + P - R, \tag{1}$$

where V is the stack volume, $\mathcal{V}$ is the bilayer volume, P is the power dissipated within the stack due to Joule heating, R is the radiative heat loss, and $\dot{Q}$ is the rate of chemical energy release per unit volume.

Note that, consistent with the small-time limit, the conductive heat flux has been ignored. In addition, thermal losses due to convection have been ignored as well, since we focus on devices triggered under vacuum. Furthermore, the present analysis also ignores the potential effect of melting of Al, Ni, or compounds thereof. Thus, the left-hand-side of Eq. (1) can be rewritten as

$$\frac{\partial H}{\partial t} = \overline{\rho C_p}\frac{dT}{dt}, \tag{2}$$

where

$$\overline{\rho C_p} \equiv \frac{\sum_{i=1}^{N} \rho^i C_p^i t^i}{\sum_{i=1}^{N} t^i}, \tag{3}$$

ρ^i, C_p^i, and t^i, respectively, denote the density, heat capacity, and thickness of the ith layer within the stack, and N is the total number of individual layers. Table I provides the values of density and heat capacity used in the computations. The emissivity values used for Pt and Al_2O_3 are 0.23 and 0.75, respectively.[20,21]

To complete the formulation, expressions must be provided for the source terms appearing on the right-hand side of the energy equation. The Joule heating term may be simply estimated from

$$P = V'I, \tag{4}$$

where V' is the applied voltage drop across the stack and I is the corresponding current. In the analysis below, both V' and I are time-dependent experimental inputs. Meanwhile, the radiative heat loss term is estimated from

$$R = \sigma(\epsilon_t A_t + \varepsilon_b A_b)\left(T^4 - T_a^4\right), \tag{5}$$

where σ is the Stefan-Boltzmann constant,[22,23] ϵ is the emissivity, A is the surface area of the stack, the subscripts t and b refer to the top and bottom surfaces, respectively, and T_a is the ambient temperature. In deriving Eq. (5), we have assumed Gray body radiation, and ignored radiative losses from the sides of the stack because the corresponding areas are substantially smaller than the horizontal surface area.

The heat of reaction is estimated using the reduced reaction formalism recently introduced in Refs. 24–26. In this model, the reaction source term is expressed in terms of stretched, normalized time variable, τ, that describes the age of the mixed Ni/Al layer. Specifically, for Ni/Al bilayers with a 1:1 ratio of the reactants, $\dot{Q}$ is expressed as[24]

TABLE I. Density and heat capacity of the materials present in the nanocalorimeter stack. The values for Al_2O_3 and SiN_x are adapted from Munro, Journal of American Ceramic Society, **80**, 1919 (1997). Copyright © 1997 The American Ceramic Society and from Riley, Journal of American Ceramic Society, **83**, 245. Copyright © 2000 The American Ceramic Society.

Material	Density (kg/m^3)	Specific heat (J/kg/K)
Aluminum	2700	904
Nickel	8908	445
Platinum	21 090	133
Titanium	4507	520
Al_2O_3	3950	1030
SiN_x	3440	877

$$\dot{Q} = \Delta\tilde{H} g(\tau) \frac{d\tau}{dt}, \tag{6}$$

where

$$\Delta\tilde{H} = \frac{\rho^{Al} C_p^{Al} + \gamma \rho^{Ni} C_p^{Ni}}{(1+\gamma)} \Delta T_f \tag{7}$$

is the heat of reaction, $\Delta T_f \simeq 1661$ K is the adiabatic flame temperature,

$$\gamma = \frac{M^{Ni} \rho^{Al}}{M^{Al} \rho^{Ni}}, \tag{8}$$

ρ^{Al}, C_p^{Al}, and M^{Al}, respectively, denote the density, heat capacity, and molecular mass of Al, ρ^{Ni}, C_p^{Ni}, and M^{Ni} denote the density, heat capacity, and molecular mass of Ni, respectively, whereas g is a canonical solution of the heat equation which is given by[24]

$$g(\tau) = 4 \sum_{n=1}^{\infty} \exp\left[\frac{-(2n-1)^2 \pi^2}{2} \tau\right]. \tag{9}$$

The evolution of the stretched time variable is governed by

$$\frac{\partial \tau}{\partial t} \equiv \frac{D(T)}{\delta^2}, \tag{10}$$

where D is the temperature-dependent atomic diffusivity. As in Ref. 24, τ is normalized using δ, the half-thickness of an Al layer, see Fig. 2. Typically, an Arrhenius dependence of D on temperature is assumed,

$$D = D_0 \exp\left(-\frac{E}{RT}\right), \tag{11}$$

and the pre-exponential factor, D_0, and activation energy, E, are obtained from fits to experimental data. As mentioned earlier, observations of the velocity of self-propagating reaction fronts have primarily been used for this purpose.[5]

Below an alternative strategy is explored based on measurements of the temperature in the nanocalorimeter stack. Before outlining this strategy, however, we note that if the atomic diffusivity and the resistive power input into the calorimeter are known, then the evolution of the temperature within the nanocalorimeter can be obtained by integrating the coupled system

$$\frac{dT}{dt} = -\frac{\Delta\tilde{H}}{\overline{\rho C_p}} \frac{\mathcal{V}}{V} g(\tau) \frac{\partial \tau}{\partial t} + \frac{V' I}{\overline{\rho C_p} V} - \frac{\sigma}{\overline{\rho C_p} V} (\epsilon_t A_t + \epsilon_b A_b)(T^4 - T_a^4), \tag{12}$$

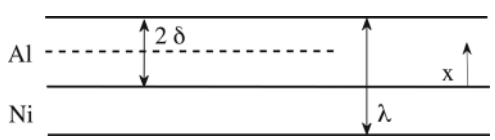

FIG. 2. Schematic illustration of a representative Al/Ni bilayer where λ is the bilayer thickness, 2δ is thickness of the aluminum layer, and x is the spatial coordinate.

$$\frac{d\tau}{dt} = \frac{D(T)}{\delta^2}. \tag{13}$$

In the computations, we integrate Eq. (13) using an explicit second-order Adams-Bashforth scheme, and Eq. (12) using an operator-split scheme where a fourth-order Runge-Kutta scheme is applied in a first fractional step in order to account for Joule heating and radiative heat loss terms, and exact integration is used in a second fractional step to account for the reaction source term.

III. INFERENCE OF DIFFUSIVITY

In this section, a simplified procedure is developed that combines the simplified thermal model developed in Sec. II with experimental measurements of temperature and power dissipation in order to infer the reaction source term and consequently the atomic diffusivity in the Ni/Al bilayer.

In order to outline the analysis, we start by rewriting Eq. (12) symbolically as

$$\dot{T} = \dot{P} + \dot{E} - \dot{R}, \tag{14}$$

where $\dot{T}$ is the heating rate of the stack, $\dot{P}$, $\dot{E}$, and $\dot{R}$ refer to the Joule heating rate, the chemical source term, and the radiation loss, respectively.

We first start by isolating heat release term, $\dot{E}$, since it directly involves the atomic diffusion rate.[24] To this end, we first note that the Joule heating rate, $\dot{P}$, is readily available from the experimental measurements, which includes the voltage drop across the stack and the current flowing through it; $\dot{P}$ follows immediately from their product. In addition, experimental data also include the measured temperature. Based on this instantaneous measurement, the radiative heat loss rate, $\dot{R}$ can be readily estimated as well. In addition, the temperature measurements can also be exploited to estimate the total heating rate, $\dot{T}$, namely, by fitting a smooth curve to the experimental data and differentiating this curve. Based on the estimates of the total heating rate, radiative loss, and Joule heating rate, the chemical source term can be estimated using Eq. (14), namely, as $\dot{E} \simeq \dot{T} - \dot{P} + \dot{R}$. Of course, several limitations arise concerning the validity of this estimate, as further discussed in Sec. IV.

Ignoring these limitations for the time being, let us assume that a suitable signal has been obtained of $\dot{E}$ versus time. One can immediately exploit this signal in conjunction with Eq. (6) in order to isolate a differential equation for $d\tau/dt$ that involves only τ and t. Integrating this differential equation yields signals of τ and $d\tau/dt$ versus time. Substituting the latter into Eq. (10) yields the desired estimates of D as a function of time or alternatively as a function of temperature. Based on this derived functional relationship, the parameters D_0 and E are estimated through a least-squares minimization procedure.

IV. RESULTS

Experimental data were obtained for two nanocalorimeter configurations, both having the same design as sketched in Fig. 1. The first configuration incorporates a Ni/Al bilayer

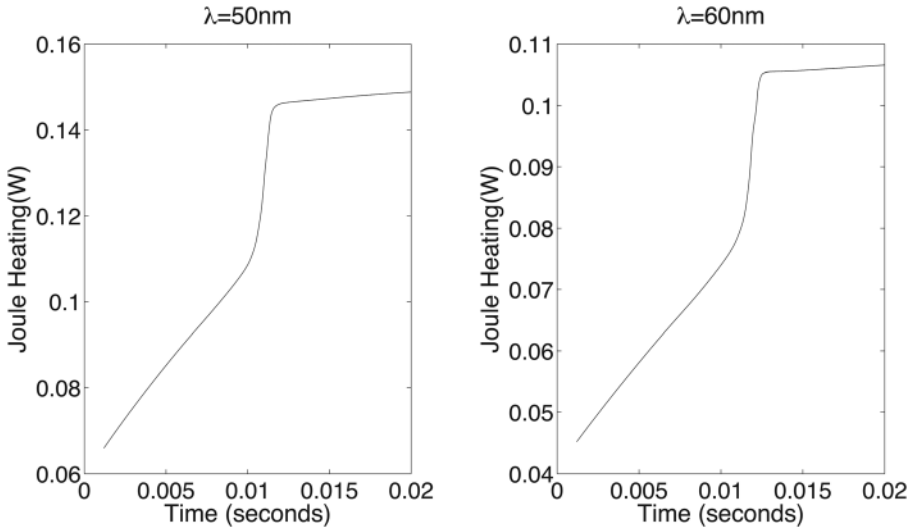

FIG. 3. Joule heating applied to the nanocalorimeter configuration for the two cases.

that is 50 nm thick, whereas the second configuration comprises a 60 nm thick bilayer. Apart from the bilayer thickness, there is also a difference in the thickness of the SiN_x layer. In the case of the 50 nm bilayer, the SiN_x layer is 100 nm thick, whereas for the 60 nm bilayer, it is 60 nm thick. As a result, the thermal mass of the device in the case of the 60 nm bilayer is smaller than that it is in the 50 nm bilayer case. This is reflected by the fact that in the initial stages of heating, the rates of temperature rise are similar for both cases, though the power dissipation is higher in the 50 nm bilayer case; see Figs. 3 and 8.

Both devices are triggered under vacuum, using a short 20 ms long capacitive discharge. The typical time constant of the circuit is 3 s, much larger than the discharge time. Figure 3 depicts the transient resistive power dissipated into the stack due to Joule heating associated with the corresponding current pulse. The curves show a rapid rise over about a 10 ms interval, following which the power dissipation remains essentially constant. The current is interrupted following the plateau depicted in the curves. Using a representative thermal diffusivity, α, of about 10^{-5} m^2/s, the thermal penetration depth corresponding to the electrical pulse duration is estimated as $\delta_t \simeq \sqrt{\alpha t_p} = 0.45$ mm. This justifies the approximations used in Sec. II, namely, that the temperature is essentially uniform within the stack over short times of order t_p.

Figure 4 shows the evolution of the heat release term, estimated from the temperature, voltage, and current measurement following the procedure outlined in Sec. III. Note that $\dot{E}$ is expected to be a positive quantity, as the mixing of Ni and Al occurs exothermically. At early and later stages, however, the estimates reveal small-amplitude negative values. These occur because at early stages, the heat release rate is small, because the temperature is low, and accordingly the mixing rates are very small. Thus, in this regime, Joule heating is essentially balanced by temperature rise and small amount of radiative heat loss. Estimates of the heat release term are consequently susceptible to noise in the measurements at very small mixing rates that are prevalent at early stages and later stages when the reaction nears completion. The fact, that at later stages the heat release term is also small, has been experimentally verified, namely, through subsequent heating steps which did not reveal any

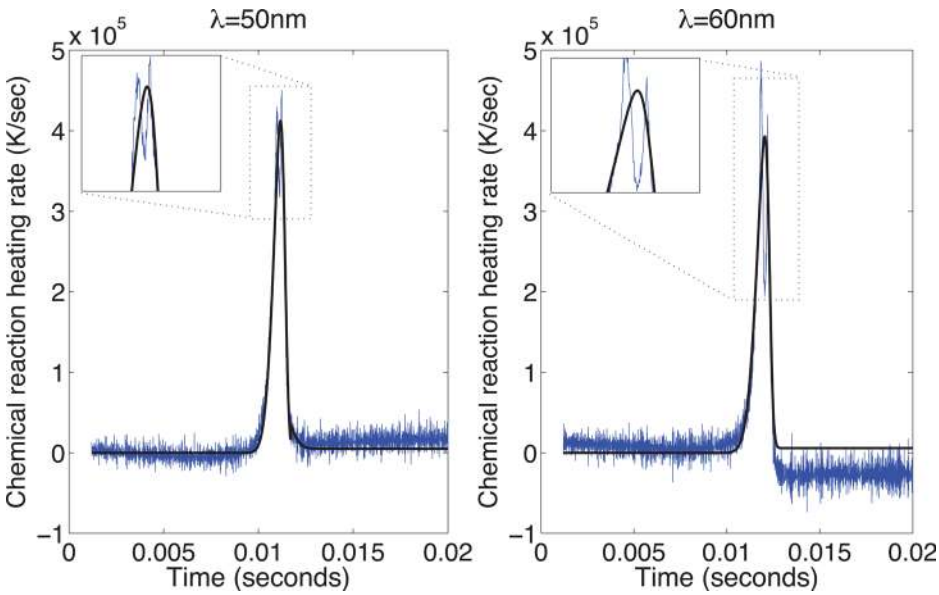

FIG. 4. (Color online) Raw data and smooth curve fit of the chemical source term in K/s. Left: $\lambda = 50$ nm; right: $\lambda = 60$ nm. Two exotherms are observed around the peak in both cases.

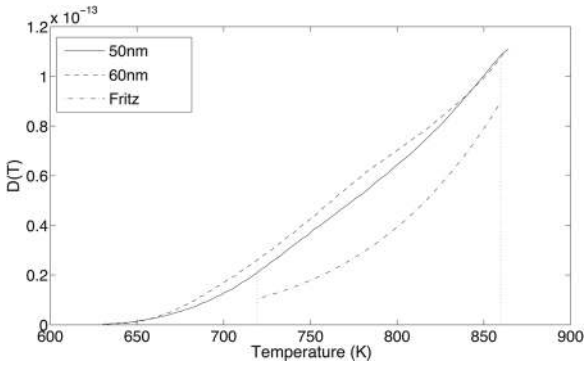

FIG. 5. Inferred diffusivity, D, vs temperature, T. Curves are generated for the 50 nm and 60 nm bilayers, as indicated. Also, shown is the extrapolated correlation of Fritz.[27]

measurable release of chemical energy. Thus, at the later stages, the estimates are also susceptible to measurement noise. In order to minimize the impact of this noise on diffusivity estimates, a smooth interpolant to the experimentally based estimates is constructed, subject to the constraint that the heat release term remains non-negative. The smooth interpolant averages the heat release rate over different phases that occur during the interdiffusion in the Ni/Al bilayer. In particular, the two neighboring peaks occurring in the experimental curve (inset of Fig. 4) are merged in the smoothing procedure. The smooth curves, which are also plotted in Fig. 4, are then used for the purpose of inferring the atomic diffusivity.

The inferred values of D are plotted against temperature in Fig. 5. Plotted are curves for the 50-nm and 60-nm bilayers. The curves are in a good agreement with each other, which indicate that the description of mixing using a Fickian approximation is consistent with the data, at least in the regime considered. As expected, D increases rapidly with T, in the range depicted. At higher values (not shown), the inferred diffusivity drops sharply, because the heat release term becomes unobservable. This may be due to potential phase change as T approaches the melting point of Al and/or the consumption of the reactants. Evidently, under these conditions, the measurement of temperature is not suitable to infer neither the heat release nor the associated mixing rate. This constitutes another limitation of the present characterization approach. In order to quantify these trends, we plot in Fig. 6 the ratio, $Z \equiv \dot{E}/\dot{P}_{\max}$, of the chemical heat release term to the peak Joule heating term associated with the electric discharge. This ratio rises rapidly from low temperatures, peaks around 860 K, and then drops rapidly at high temperatures. Clearly, the estimated heat release is least susceptible to measurement noise when Z is large. In particular, values $Z > 2$ would conservatively ensure that the chemical heat release is a dominant contributor to the observed temperature rise, and consequently that the estimates are least affected by measurement noise or cancellation errors. Based on the results in Fig. 6, $Z > 2$ for temperatures ranging from 720 K to 860 K. A rapid decrease in the heat release is observed beyond 860 K as the reaction nears completion. Consequently, this temperature regime is considered to be optimal for estimating the diffusion parameters for the interdiffusion in the Ni/Al bilayer. A similar observation is made for the 60 nm bilayers; the corresponding results are consequently omitted.

We further analyze the dependence of D on temperature by plotting the natural logarithm of the diffusivity against T^{-1}. Figure 7 shows curves of $\ln(D)$ generated for both bilayers, with the temperature restricted to the range of 720–860 K. A straight line fit to the data is also depicted in the plot. Over the temperature range considered, the data may be closely approximated by a straight line, which indicates that an Arrhenius correlation is suitable. The corresponding values of the pre-exponent and activation energy are $D_0 = 2.79 \times 10^{-10}$ m^2/s and $E = 57.37$ kJ/mol.

Of course, it would have been ideal to conduct direct comparison of the presently inferred values with other estimates obtained by independent measurement techniques. Unfortunately, for the present range of temperatures, direct measurements are not readily available. In general, estimates of Ni/Al interdiffusion rates at temperatures that are high enough for reactions to initiate but smaller than the melting temperature of Al remain quite scarce. Recently, however, Fritz[27] attempted to estimate diffusion rates based on an experimental analysis of the ignition temperature and ignition thresholds of nanostructured Ni/Al bilayers. The

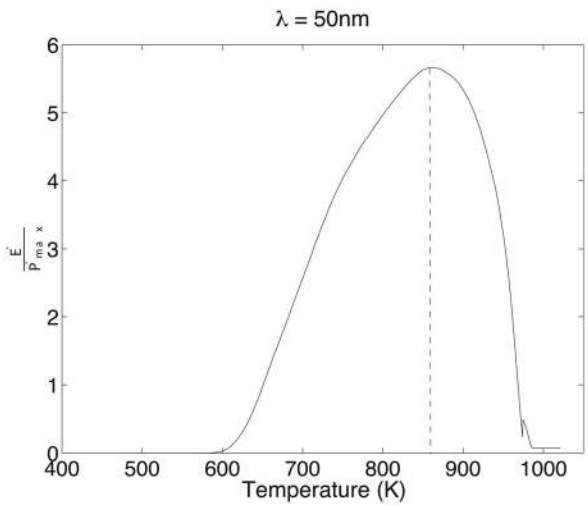

FIG. 6. Ratio of the chemical heat release rate to the maximum Joule heating rate vs temperature. Plotted are results obtained for $\lambda = 50$ nm.

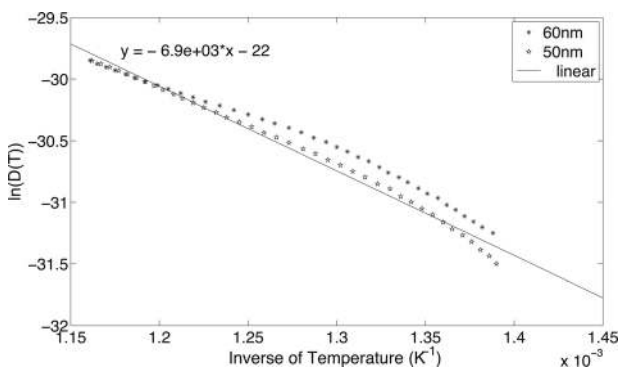

FIG. 7. Natural logarithm of D plotted against T^{-1}. Curves are generated for the 50 nm and 60 nm bilayers, as indicated.

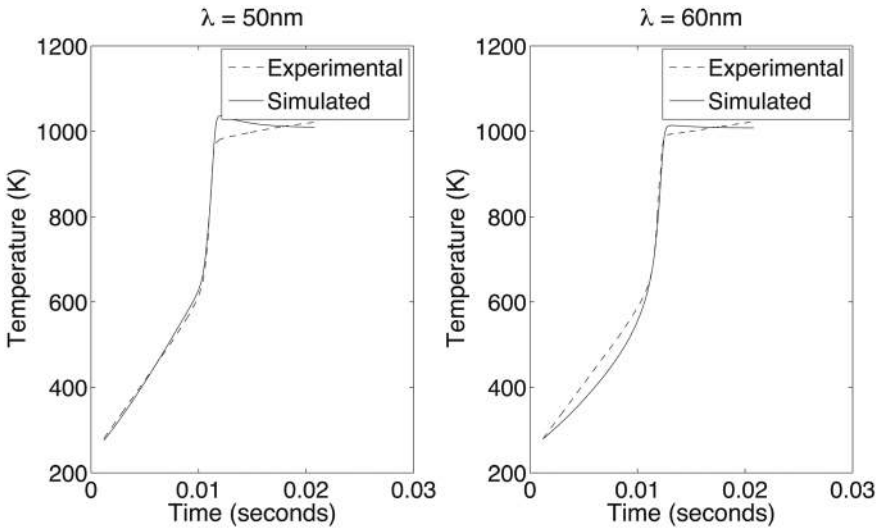

FIG. 8. Temperature vs time for $\lambda = 50$ nm (left) and 60 nm (right). Plotted are curves depicting a comparison between raw experimental data and simulated results.

experimental correlation resulting from Fritz's analysis is also plotted in Fig. 5. Though quantitative differences between Fritz's correlation and the present estimates are evident, the consistency between the estimates and the overall trends is encouraging.

In order to verify the present diffusivity estimates, we substitute the Arrhenius correlation derived from Fig. 7 into the governing equations (12) and (13) and perform the integration. Since data are not available for $T < 720$ K, the correlation obtained by Fritz[27] is used for this temperature range. For the same reason, the presently inferred Arrhenius correlation is simply extrapolated to higher temperatures. The experimental measurement of the Joule heating term is used as input to the calculations, but all other variables are computed in the model based on known dimensions and thermophysical properties. Figure 8 shows the evolution of the computed temperature during and following the application of the electrical stimulus. Plotted are curves for the 50 nm and 60 nm bilayers; the corresponding experimental temperature measurements are also shown for comparison. For both cases, a very close agreement is observed between simulation results and measured data. This supports the validity of the diffusivity estimates at least in the intermediate temperature range where the chemical heat release term is large.

To further verify the present predictions, Fig. 9 compares the experimentally inferred and computationally determined heat release rates for both the 50 nm and 60 nm bilayers. As observed for temperature, the experimental and computational curves for the heat release term are in close agreement, at intermediate times when the magnitude of the heat release is large. Within the corresponding range of temperatures, this agreement further supports the inferred diffusivity estimates.

Finally, we examine the assumption made in the analysis that complete mixing occurs when the nanocalorimeter is triggered with a sufficiently strong electric stimulus. To this end, we once again rely on the experimental measurements, which subjected the same nanocalorimeter to multiple, nominally identical electric stimuli and monitored the subsequent rise and decay of the temperature. The experimental observations showed the temperature response of the nanocalorimeter were essentially identical following the first stimulus,

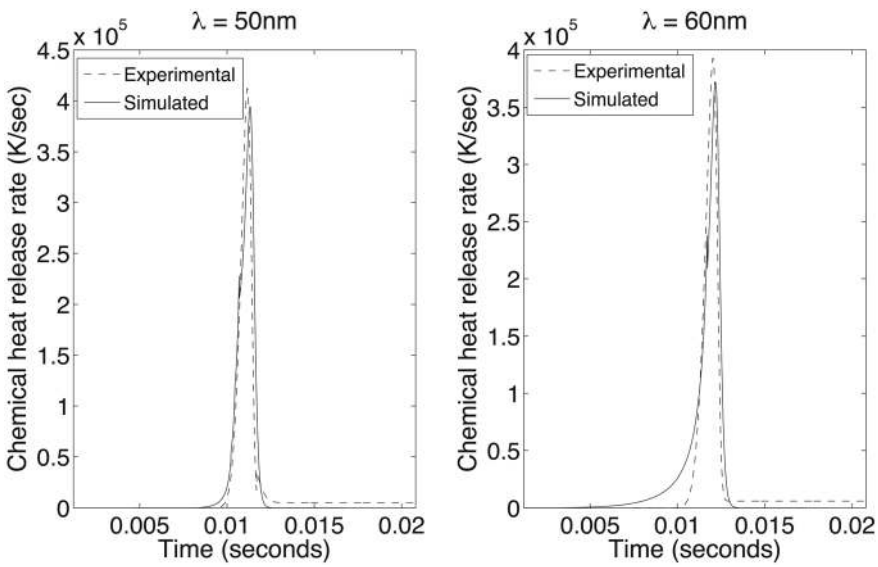

FIG. 9. Chemical source term vs time for $\lambda = 50$ nm (left) and 60 nm (right). Plotted are curves depicting experimental and simulation results, as indicated.

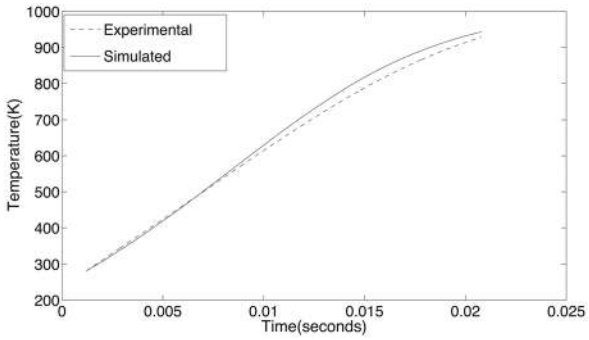

FIG. 10. Evolution of the temperature for $\lambda = 50$ nm. Plotted are experimental data obtained using the nanocalorimeter after the first initiation as well as simulation results obtained by omitting the chemical source term.

which indicates that under the present conditions, no significant exothermic energy release occurs following the first experimental test. To further verify this claim, we have performed simulations of an "inert" nanocalorimeter, namely, by integrating Eq. (12) with the first term omitted. Figure 10 compares the results of these simulations with the experimental temperature curves obtained for the second test. An excellent agreement between the experimental and computational curves can be observed. This further supports the assumption that mixing is complete during the first test and lends confidence in our thermal radiation loss model.

V. CONCLUSIONS

A computational model was developed to describe the evolution of the temperature field in a nanocalorimeter that comprises inert layers on which a Ni/Al bilayer is deposited. The model incorporates a reduced continuum description of mixing and heat release in the Ni/Al bilayer, and of the energy equation in the inert layers. Due to the small thicknesses of individual layers that are several orders of magnitude smaller than the corresponding length, a simplified, transient, homogeneous representation of the temperature field was adopted. The resulting lumped model is valid over short enough timescales, which are nonetheless sufficiently large to capture the formation reaction. Attention is focused on nanocalorimeters triggered electrically under vacuum, so that the global energy balance accounts for the effects of Joule heating, chemical heat release, and radiative heat losses.

By using experimental observations of the evolution of the temperature, the computational model is used to estimate the transient heat release rate. Assuming an Arrhenius model for the mixing between Ni and Al, the estimated heat release rate is then used to determine the pre-exponent and activation energy in the corresponding correlation for the atomic diffusivity. The model is applied to analyze experimental observations of the response of two nanocalorimeter configurations, the first 50 nm Ni/Al bilayer, whereas the second comprises a 60 nm Ni/Al bilayer. In both cases, the nanocalorimeter is triggered using a short electrical discharge, and the experimental observations included the evolution of the current and voltage drop across the device as well as the temperature. Each nanocalorimeter was triggered multiple times, particularly to verify that the heat of reaction is released during the first test. Thus, experimental data included the response of both "live" and "spent" devices.

Application of the computational model to analyze experimental observations of both nanocalorimeter configurations indicates that:

1. The predicted values of the diffusivity obtained from the 50 nm and 60 nm configurations are consistent with each other. Thus, the simplified description of interdiffusion appears to be consistent with the experimental observations, at least in the regime considered.
2. Limitations to the present analysis arise (a) at lower temperatures, due to the low magnitude of the heat release term, and (b) at higher temperatures, due to phase-change effects and/or the rapid drop in heat release as reactants are consumed. In both cases, the heat release rate is susceptible to measurement noise and is consequently unobservable. For the present setting, the diffusivity was reliably extracted for an intermediate temperature range extending from about 700 K to 860 K.
3. A very good agreement was observed between the temperature field simulated using inferred diffusivity and the experimental observations, and between the simulated and experimentally inferred heat release rates. Excellent agreement was also observed between the simulated and observed thermal response of the spent device.

Overall, the present experiences indicate that nanocalorimetric measurements appear to provide a promising means of characterizing atomic diffusion rates. Work is underway to generalize the scope of the present model, namely, by accounting for phase change effects, and for convective and conductive heat losses.

ACKNOWLEDGMENTS

Research supported by the U.S. Department of Energy, Office of Basic Energy Sciences, Division of Materials Sciences and Engineering under Award No. DE-SC0002509.

[1]A. F. Lopeandia, J. Rodriguez-Viejo, M. Chacon, M. T. Clavaguera-Mora, and F. J. Munoz, J. Micromech. Microeng. **16**, 965971 (2006).
[2]R. K. Kummamuru, L. de la Rama, L. Hu, M. D. Vaudin, M. Y. Efremov, M. L. Green, D. A. LaVan, and L. H. Allen, Appl. Phys. Lett. **95**, 181911 (2009).
[3]P. Swaminathan, M. Grapes, S. C. Barron, D. A. LaVan, and T. P. Weihs, J. Appl. Phys. (to be submitted).
[4]C. Michaelsen, K. Barnak, and T. P. Weihs, J. Phys. D: Appl. Phys. **30**, 3167 (1997).
[5]A. B. Mann, A. J. Gavens, M. E. Reiss, D. Van Heerden, G. Bao, and T. P. Weihs, J. Appl. Phys. **82**, 1178 (1997).
[6]M. E. Reiss, C. M. Esber, D. Van Heerden, A. J. Gavens, M. E. Williams, and T. P. Weihs, Mater. Sci. Eng., A **261**, 217 (1999).
[7]E. Ma, C. V. Thompson, L. A. Clevenger, and K. N. Tu, Appl. Phys. Lett. **57**, 1262 (1990).
[8]T. S. Dyer, Z. A. Munir, and V. Ruth, Scr. Metall. **30**, 1281 (1994).
[9]T. P. Weihs, A. J. Gavens, M. E. Reiss, D. Van Heerden, A. E. Draffin, and D. Stanfield, in *Chemistry and Physics of Nanostructured and Related Non-Equilibrium Materials*, edited by E. Ma, B. Fultz, R. Shull, J. Morral, and P. Nash (TMS, Warrendale, PA, 1997).
[10]T. P. Weihs, *Handbook of Thin Film Process Technology* (IOP, Bristol, United Kingdom, 1998), Part B, Section F 7.
[11]A. S. Rogachev, Russ. Chem. Rev. **77**, 21 (2008).

[12]A. J. Gavens, D. Van Heerden, A. B. Mann, M. E. Reiss, and T. P. Weihs, J. Appl. Phys. **87**, 1255 (2000).
[13]S. Jayaraman, A. B. Mann, O. M. Knio, G. Bao, and T. P. Weihs, in *Proceedings of the MRS Symposium*, edited by E. Ma, M. Atzmon, P. Bellon, and R. Trivedi (Materials Research Society, Warrendale, PA, 1998), Vol. 481, p. 563.
[14]S. Jayaraman, A. B. Mann, T. P. Weihs, and O. M. Knio, Proc. Combust. Inst. **27**, 2459 (1998).
[15]S. Jayaraman, O. M. Knio, A. B. Mann, and T. P. Weihs, J. Appl. Phys. **86**, 800 (1999).
[16]S. Jayaraman, A. B. Mann, M. Reiss, T. P. Weihs, and O. M. Knio, Combust. Flame **124**, 178 (2001).
[17]E. Besnoin, S. Cerutti, O. M. Knio, and T. P. Weihs, J. Appl. Phys. **92**, 5474 (2002).
[18]R. Knepper, M. R. Snyder, G. Fritz, K. Fisher, O. M. Knio, and T. P. Weihs, J. Appl. Phys. **105**, 083504 (2009).
[19]L. Alawieh, O. M. Knio, and T. P. Weihs, J. Appl. Phys. **110**, 013509 (2011).
[20]R. G. Munro, J. Am. Ceram. Soc. **80**, 1919 (1997).
[21]F. L. Riley, J. Am. Ceram. Soc. **83**, 245 (2000).
[22]J. Stefan, in proceedings of the Mathematics and Science Class of the Imperial Academy of Sciences Vol. 79 (Vienna 1879), pp. 391–428.
[23]L. Boltzmann, Annalen der Physik **258**, 291 (1884).
[24]M. Salloum and O. M. Knio, Combust. Flame **157**, 288 (2010).
[25]M. Salloum and O. M. Knio, Combust. Flame **157**, 436 (2010).
[26]M. Salloum and O. M. Knio, Combust. Flame **157**, 1154 (2010).
[27]G. M. Fritz, Ph.D. dissertation (The Johns Hopkins University, 2011).